MINERALOGICAL MAGAZINE, JUNE 1972, VOL. 38, PP. 693–711

The crystal structure of stilpnomelane. Part II. The full cell

R. A. EGGLETON

Department of Geology, Australian National University, Canberra, A.C.T., Australia

SUMMARY. The structural formula of stilpnomelane averaged from 37 representative literature analyses and based on the determined structure is $(Ca,Na,K)_4(Ti_{0\cdot1}Al_{2\cdot3}Fe_{35\cdot5}Mn_{0\cdot8}Mg_{9\cdot3})[Si_{63}Al_9](O,OH)_{216}.nH_2O$. Ferrostilpnomelanes have up to 12 R^{3+} cations in the octahedral sheet, ferristilpnomelanes commonly have between 24 and 30 R^{3+} cations, rarely up to 37. The two groups can be distinguished by accurate X-ray powder diffraction, ferrostilpnomelanes having d_{001} less and a greater than have ferristilpnomelanes. The unit cell is triclinic, $a = b \sim 21{\cdot}8$ Å, $\gamma = 120°$, $d_{001} \sim 12{\cdot}2$ Å, $P\bar{1}$. Hexagonal groups or 'islands' of 24 silicon–oxygen tetrahedra co-ordinate to the octahedral sheet, the centres of the 'islands' are displaced by $5a/12$, $8b/12$ on either side of the octahedral sheet as a result of warping of this sheet to permit articulation with the smaller tetrahedral sheet. The 24-tetrahedra 'islands' are linked laterally by 6-member rings of inverted tetrahedra, which in turn link at their apices to like rings connecting the next sheet of 'islands'. Thus a single tetrahedral layer is 4 tetrahedra thick and has symmetry $6/m$. The 6-member rings of tetrahedra act as hinges permitting up to 0·5 Å extension or contraction of the tetrahedral sheet to accommodate variations in the octahedral sheet dimensions with varying R^{2+}/R^{3+} ratio.

IN Part I of this study (*The Subcell*, Eggleton and Bailey, 1965) it was shown that stilpnomelane was triclinic with $a = b = 21{\cdot}72$ Å, $c = 17{\cdot}74$ Å, $\alpha = 124°$, $\beta = 96°$, $\gamma = 120°$. A subcell having a_s and b_s one quarter of the true a and b dimensions was defined, and the crystallography, composition, and average structure of the subcell was described. The composition of the subcell as revealed by the present study is $A_{<1}R^{vi}_3T^{iv}_{4\cdot5}(O,OH)_{13\cdot5}.nH_2O$.

Since Part I was published, additional analysed samples of stilpnomelane have generously been made available to the author, and other workers (e.g. Blake, 1965; Brown, 1967; Smith and Frondel, 1968; Rost and Stettner, 1969; Hashimoto, 1969; Häberle, 1969; and Kräutner and Medeşan, 1969) have added data and discussion to the problems of the stilpnomelane group. This paper reports the determination of the full structure, and relates the variations in composition and cell dimensions to the structure. The ideal structure of the stilpnomelane tetrahedral sheet has been briefly reported elsewhere (Eggleton, 1970).

Nomenclature. Hutton (1938) proposed that stilpnomelane in which the bulk of the iron was ferrous be called ferrostilpnomelane, the name stilpnomelane being retained for the ferric-iron rich variety. Several writers (e.g. Katada and Sumi, 1966; Brown, 1967; and Hashimoto, 1969) have used 'ferristilpnomelane' in place of Hutton's use of stilpnomelane *sensu stricto*. It is proposed here to adopt this nomenclature, leaving 'stilpnomelane' as a general term for the group as a whole.

Symmetry. In Part I, significantly better agreement between observed and calculated structure factors was achieved using a non-centrosymmetric model, in agreement with the results of the $N(z)$ statistical test on the subcell reflections. The deviation from centrosymmetry was not great, amounting to little more than a difference in the z-co-ordinates of otherwise equivalent atoms on either side of the octahedral sheet.

The superlattice reflections show a centrosymmetric distribution of intensity (fig. 2) and this symmetry has been assumed for stilpnomelane. If it is assumed that over the full cell 'planes' of atoms are not strictly planar, the variations in z-co-ordinate which resulted from the non-centrosymmetric subcell model can be accommodated while retaining a centre of symmetry for the full cell.

Determination of model structure

Superlattice reflections. The X-ray reflections from stilpnomelane are of 3 types, referred to here (and in Part I) as T1, T2, and T3 reflections. T1 reflections are the subcell reflections. They are strong, sharp, and show trigonal symmetry. The T2 and T3 reflections define the true triclinic cell and together can be referred to as superlattice reflections. T2 reflections are weaker than T1 and in most stilpnomelane crystals reveal stacking disorder, being elongated parallel to c^*. The T2 reflections from the crystal used in this study (described in detail in Part I) only show slight elongation. T3 reflections are weak but sharp and have indices $12n\pm1,12n\pm1,l$ ($n = 0,1,2,...$). Thus they occur in rows parallel to c^* on either side of the rows of T1 reflections. The subcell structure was determined using only the T1 reflections, but because these reflections give no information about the differences between subcells, detail in the stilpnomelane structure could not be determined.

The T2 reflections show pseudo-trigonal symmetry, and recognition of this property led to the determination of the full-cell structure. Eggleton (1969) has shown that a symmetric atom group arranged in an asymmetric lattice produces a diffraction pattern from which the Fourier transform of the atom group may be elucidated. Only pseudo-reflection symmetry was described in that study, although the extension to pseudo-rotation symmetry is obvious.

A reciprocal lattice row (for example $40l$) provides point samples of the Fourier transform of the unit cell. The interval between sample points ($= c^*$ in this case) is of the same order of magnitude as the distance between nodes in the transform and hence it is in general not possible to deduce the continuous function from such sparse samples. If, however, the transform has rotation symmetry but the lattice does not, elsewhere a second reciprocal lattice row (for example $04l$) will provide different point samples of the symmetry-equivalent continuous function. Artificial superposition of the two rows thus doubles the sample density.

The stilpnomelane reciprocal lattice rows $40l$, $04l$, and $\bar{4}4l$ fulfil the requirement of giving different point samples of symmetry-equivalent regions of the Fourier transform. Superposition of the data from each row clearly shows the continuous variation in scattering that would be observable if a single unit cell could be X-rayed (fig. 1).

It was assumed from the outset that the octahedral sheet makes little or no contribution to the T2 reflections, and therefore that these reflections arise solely from the

tetrahedral region. Using this assumption, the real and pseudo-symmetry of the T2 reflections give the symmetry of the tetrahedral arrangement. Application of the $N(z)$ test for centrosymmetry (Howells, Phillips, and Rogers, 1950) to the superlattice reflections shows a centrosymmetric distribution (fig. 2). This symmetry and the layer nature of stilpnomelane suggest that the point symmetry of the tetrahedral layer is at least as high as $6/m$. However the crystal as a whole is triclinic and to make best use of the high symmetry of the tetrahedral region the structure of a tetrahedral sheet was considered in isolation from the crystal as a whole. The ideal tetrahedral structure was determined by simulating the X-ray diffraction data by optical diffraction.

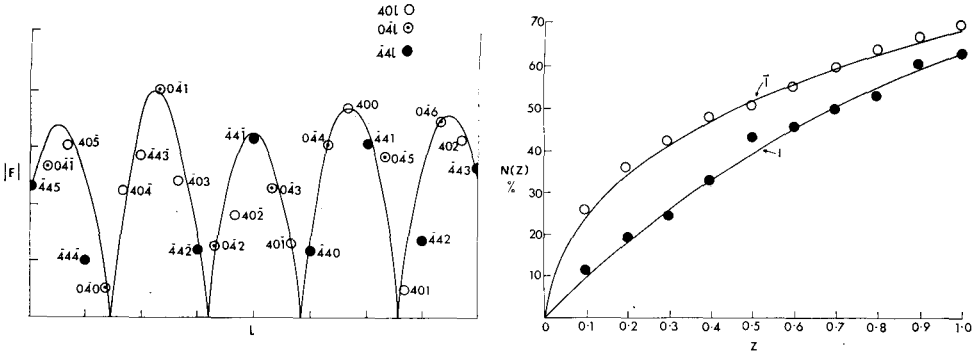

FIGS. 1 and 2: FIG. 1 (left). Structure amplitudes of $04l$ and pseudo-symmetric equivalent reflections $40l$, $\bar{4}4l$. FIG. 2 (right). Test for centrosymmetry (after Howells *et al.*, 1950). Open circles, T2 and T3 reflections; full circles, T1 reflections.

An *optical diffractometer* was constructed following the description given by Taylor and Lipson (1964), but replacing the pinhole coherent light source with a 0·4 milliwatt He–Ne laser. The high intensity of this source allowed experimental procedures to be greatly simplified. The diffractometer was set up horizontally, the components being mounted on unconnected optical benches. Alignment of the lenses is rapid, as multiple reflection images of the source are seen when a lens is out of alignment, and concentric interference rings appear when the alignment is true. The diffraction pattern can be projected on a screen at any desired enlargement, or recorded directly on film. An exposure of 1/500 sec. using ordinary black and white film was found to be adequate for recording all but the weakest patterns, thus the instrument needed no protection against vibration.

The models tested were made by punching holes of diameter proportional to scattering factors of the atoms concerned in old X-ray film. A 10 to 1 reducing pantograph punch was made following the outline given by Taylor and Lipson (1964). Although holes of differing size do not accurately simulate atoms of differing atomic number, the error introduced at low angle is slight. The scale of the model (about 1 mm. = 1 Å) was chosen to keep that part of the diffraction pattern of interest well within the first diffraction minimum from the largest hole punched. The punch mechanism used was a fixed punch having a rotating eccentric die with 7 hole sizes (0·5, 0·625, 0·75, 1·0, 1·25, 1·5, and 2·0 mm.) and having interchangeable punches.

Interpretation of T2 reflections. Determination of the tetrahedral sheet structure began with consideration of the strongest T2 reflections 40*l* and 80*l* and with their pseudo-symmetric equivalents 04*l*, $\bar{4}4l$ and 08*l*, $\bar{8}8l$. Fig. 3 shows a triple exposure of the reciprocal lattice planes 0*kl*, *h*0*l*, $\bar{h}hl$ and is in effect the Fourier transform of the tetrahedral sheet. Examination of the row having $h,k = 4$ shows a periodicity of zero intensity of 0·9*l*. Assuming a sign change at zero intensity, the true periodicity of this row is about 1·8*l*. This intensity variation can be attributed to a pair of atoms separated by $z = 0{\cdot}56$. (It should be noted here that while neither '*l*' nor '*z*' have any absolute significance for a single tetrahedral sheet, the crystal as a whole provides a convenient reference scale in both direct space (c) and in reciprocal space (c^*) and so 'crystal scale' will be used throughout this discussion.) The postulated atom pair with z separation 0·56 must repeat at regular intervals along y in order to produce a 'one-dimensional crystal' in agreement with the one-dimensional diffraction pattern being considered.

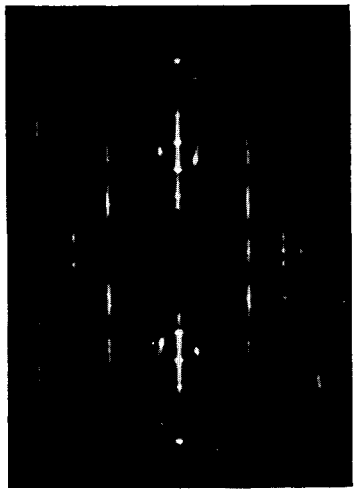

FIG. 3. Precession photograph of stilpnomelane, 0*kl*, *h*0*l*, $\bar{h}hl$ triple exposure.

A similar analysis suggests that the row having $h,k = 8$ might be explained by atoms separated by $z = 0{\cdot}21$. However atoms that contribute to rows with $h,k = 4$ must also contribute to rows with $h,k = 8$ (although the reverse need not apply); therefore the periodicity of this row must be explained in terms of the addition of two periodic functions. Examination of the row with $h,k = 8$ shows that the intensity is not strictly periodic over the observable region, strengthening the argument that the row results from the addition of 2 functions. A distribution close to that observed can be achieved by adding the contributions of silicons at $z = \pm 0{\cdot}28$ to that of oxygen at $z = 0{\cdot}23$. The co-ordinates so determined are consistent with those found for the tetrahedral atoms in the subcell structure (after an origin shift of $c/2$).

The next most intense reciprocal lattice row is that having $h,k = 6$. The variation in intensity of this row can be explained by atoms separated by $z = 0{\cdot}24$, that is, having co-ordinates $z = \pm 0{\cdot}12$. These co-ordinates were interpreted as locating the silicons of the inverted tetrahedra. The remainder of the tetrahedral sheet was deduced from co-ordination considerations and from the rest of the Fourier transform. Fig. 4 shows the optical diffraction mask representing the ideal model of the tetrahedral sheet viewed in [110] projection, and the optical diffraction pattern of this mask. The pattern can be compared with the X-ray diffraction pattern of stilpnomelane shown in fig. 3.

Description of the model structure. An iron-bearing octahedral sheet has lateral dimensions too large to permit articulation of a continuous hexagonal sheet of silicon tetrahedra. For example, the 'rectified wave' model for antigorite has articulation

between the sheets maintained for about 20 Å (Kunze, 1956); in zussmanite articulation is only maintained over one 6-member ring of tetrahedra (Lopes-Vieira and Zussman, 1969). In stilpnomelane co-ordination between octahedral and tetrahedral sheets is maintained over a distance of 7 linked tetrahedra, giving a group of 24 tetrahedra linked together in a hexagonal array, and co-ordinating to the octahedral sheet. Such groups of tetrahedra will be hereafter referred to as 'islands'. The 'islands' are linked together by 6-member rings of tetrahedra, having their apices pointing in the opposite direction to those of the 'islands'. The apices of the 6-member rings serve

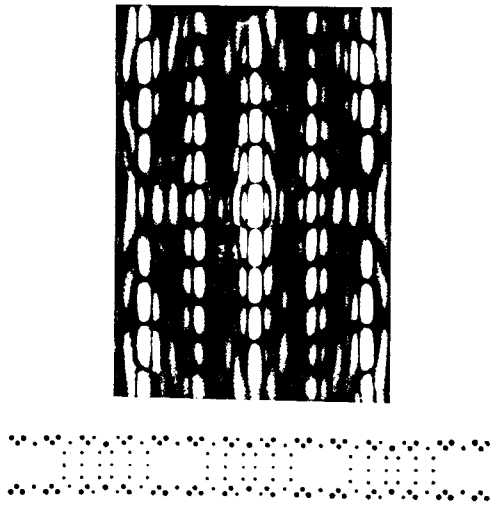

FIG. 4. Optical diffraction (above) of the mask (below) used for simulation of the stilpnomelane tetrahedral sheet, [110] projection.

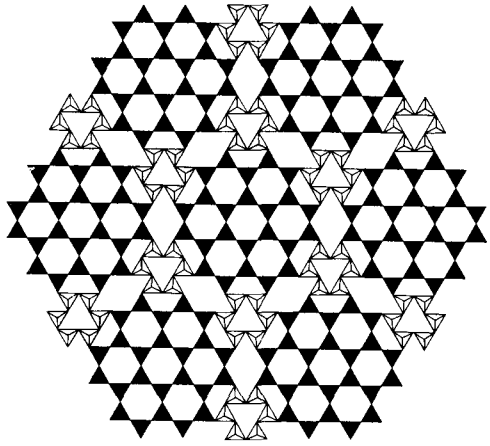

FIG. 5. Vertical (c^*) projection of the stilpnomelane tetrahedral sheet. Solid triangles, tetrahedra co-ordinated to the octahedral sheet; outline tetrahedra, 6-member rings linking 'islands' of tetrahedra.

also as the apices of like but inverted 6-member rings, which in turn link the 'islands' co-ordinating to the next octahedral sheet. The 'islands' and 6-member rings form 5-member rings at their junction (figs. 5 and 11). This model has composition $Fe_{48}Si_{72}(O,OH)_{216}$.

Determination of the actual structure

Powder diffraction patterns have been obtained for 13 stilpnomelanes; details of the samples are given in Table I. All powder patterns were obtained with a 114·6 mm Debye-Scherrer camera, using Mn-filtered Fe-radiation. Line positions were referred to an Si internal standard.

Cell dimensions were determined by least-squares refinement of the strong (T1) reflections. The results are plotted in fig. 6 as a *vs.* d_{001}. In calculating cell dimensions, it was assumed that $a = b$ and $\gamma = 120°$, that is, the pseudo-trigonal nature of the subcell was utilized. Thus for the T1 reflections there are in effect only 2 variables, a and d_{001}. A list of d-spacings for ferrostilpnomelane is given in Table II.

All the lines observed on stilpnomelane powder photographs can be indexed on the basis of the triclinic cell described in Part I, and no evidence has been found for polytypism. It can be seen from fig. 6 that a is greatest and d_{001} is least for ferrostilpnomelane, and that a is least and d_{001} greatest for ferristilpnomelane.

Effect of heat on stilpnomelane. Hutton (1938) and Armstrong (Gruner, 1937) have shown that as stilpnomelane is heated there is a continual weight loss up to about

TABLE I

Sample	Location	Analysis	Collected by	Comment
A	Crystal Falls, Minnesota	36	Author	From the same locality as analysed material
B	French Ridge, New Zealand	—	Univ. of Otago	—
C	Queenstown, W. Otago, New Zealand	—	A. E. Grady	From the same locality as analysed material
D	Poplar Creek, British Columbia	25	P. Read	Part of rock from which analysed sample was extracted
E	Cobar, N.S.W.	21	I. M. Threadgold	Part of analysed material
F	Cuyuna Range, Minnesota		S. W. Bailey	Appears identical with sample G
G	Cuyuna Range, Minnesota	18	R. Blake	Part of analysed material
H		11		Part of analysed material
I		13		Part of analysed material
J	Auburn Mine, Minnesota	—	J. Lister	Pale green rosettes in vugs in quartz
K	Franklin, New Jersey	42	C. Frondel	Part of analysed material
L	Queenstown, New Zealand	35	A. E. Grady	From the same locality as analysed material
M	Hamersley Ranges, Western Australia	1	G. L. LaBerge	Part of analysed material

350°. This weight loss was attributed to both the loss of absorbed and interlayer water, and the loss of (OH) as ferrous iron oxidized. Kräutner and Medeşan (1969), in a more detailed study of weight loss on heating, find a loss equivalent to 4(OH) (based on 8(Si+Al) in the unit cell) after 450 °C. This amount corresponds to all the octahedral (OH) in the sample (35·5(OH) based on 72(Si+Al), analysis 14, Table IV).

D.T.A. curves of stilpnomelane from the Cuyuna Range, Minnesota (sample F, Table I), were obtained using a Rigaku-Denki instrument, model DTAA3/020164, with a heating rate 10°/minute. They show a strong endotherm from room temperature to about 150° and a second weak endotherm spread from 150° to 440°, at which

temperature a sharp exotherm occurs. A second sharp exotherm begins at about 800° (Fig. 7). Kräutner and Medeşan report a similar D.T.A. curve.

As described in the section on powder diffraction data, d_{001} varies with Fe^{3+}/Fe^{2+} ratio; for the one sample, d_{001} can therefore be used to detect changes in this ratio during heating. Fig. 7 shows d_{001} plotted against temperature for sample F. The basal

TABLE II. *X-ray powder data of ferrostilpnomelane (sample L, Table I).*

hkl†	d_{meas}	d_{calc}	I/I_0	Type	*hkl*†	d_{meas}	d_{calc}	I/I_0	Type
001	12·1 Å	12·1 Å	>10	T1	$44\bar{1}$	2·1889	2·1892	3	T1
$01\bar{2}$	8·2	8·2	B	T3	$44\bar{8}$	2·1109	2·1101	5	T1
$11\bar{2}$					440	1·956	1·957	2	T1
$1\bar{2}0$					$44\bar{9}$	1·8856	1·8847	4	T1
$12\bar{2}$	7·16	7·12	B	T2, T3	4.4.$\bar{1}$0	1·685	1·685	4	T1
$10\bar{2}$					12.0.$\bar{5}$	1·5853	1·5844	6	T1
etc.					12.0.$\bar{6}$	1·5715	1·5710	5	T1
002	6·07	6·05	1	T1	12.0.$\bar{4}$				
$24\bar{2}$	5·48	5·48	2	T2	12.0.$\bar{7}$	1·5324	1·5327	2	T1
$1\bar{2}1$					12.0.$\bar{3}$				
$22\bar{2}$					4.4.$\bar{1}\bar{1}$	1·5138	1·5139	3	T1
$04\bar{3}$	4·75	4·73	3	T2	443	1·4141	1·4141	2	T1
$44\bar{1}$					12.0.$\bar{9}$	1·4037	1·4036	1	T1
Many	4·13	—	2	T2	12.0.$\bar{1}$				
003	4·039	4·033	8	T1	$88\bar{8}$	1·3674	1·3683	2	T1
$01\bar{4}$	3·6	—	B	T2	$88\bar{7}$	1·3484	1·3483	3	T1
etc.					8.8.$\bar{1}\bar{1}$	1·325	—	2	T1
004	3·027	3·025	7	T1	12.0.0				
$44\bar{5}$	2·715	2·713	4	T1	12.0.$\bar{1}$0				
$44\bar{6}$	2·570	2·567	10	T1	444	1·2834	1·2835	3	T1
$44\bar{2}$	2·431	2·426	2	T1	$88\bar{3}$	1·154	1·154	2B	T1
$44\bar{7}$	2·350	2·348	7	T1	8.8.$\bar{1}$6	1·055	1·055	1	T1

† Also the pseudo-symmetric equivalent reflections (k, $\overline{h+k}$, $13h/3+11k/3+l$), ($\overline{h+k}$, $\overline{h+2k}$, $2h/3+13k/3+l$) for the T1 reflections.
B broad reflection.
Reflections used in least-squares refinement of cell parameters are listed to 4 decimal places. $a = 21{\cdot}955 \pm 0{\cdot}022$, $b = 21{\cdot}955 \pm 0{\cdot}022$, $c = 17{\cdot}619 \pm 0{\cdot}022$, $d_{001} = 12{\cdot}100$, $\alpha = 124{\cdot}83° \pm 0{\cdot}01$, $\beta = 95{\cdot}96° \pm 0{\cdot}01$, $\gamma = 120°$.

spacing was determined from the average of $3d_{003}$ and $4d_{004}$ measured using Cu-$K\alpha$ radiation on a Philips P.W. 1050/30 diffractometer with pulse height discrimination. d_{001} begins to increase between 120 °C and 150 °C and has reached its maximum value after heating at 230 °C for 16 hours. The rate of change is dependent on grain size, crushed but unground material showing two peaks in the diffraction pattern at each position, one remaining near the room temperature value up to 500 °C, the other increasing after heating beyond 150 °C.

As is shown in the next section, the octahedral cations in stilpnomelane fall into three groups. A group of 12 that are easily oxidized, a group of 18 that require a higher oxidation potential before they oxidize, and a further group of 18 which are extremely difficult to oxidize. The D.T.A., thermo-gravimetric, and diffraction data

may be interpreted [following Blake (1964) and Kräutner and Medeşan (1969)] as: 20°–150°, loss of absorbed interlayer water; 150°–350°, oxidation of up to 12 Fe^{2+} cations, loss of equivalent structural (OH) and more interlayer water; 400°–500°, rapid oxidation of a further 18 Fe^{2+} cations, loss of equivalent 18(OH), increase in d_{001}; 500°–800°, slow oxidation of any unoxidized Fe^{2+}, loss of remaining (OH) (18 maximum); 800°–50°, breakdown of stilpnomelane.

The diffraction data indicate that this interpretation may only apply under the comparatively rapid heating rate of the equipment used and should not be regarded as providing a geothermometer at this stage.

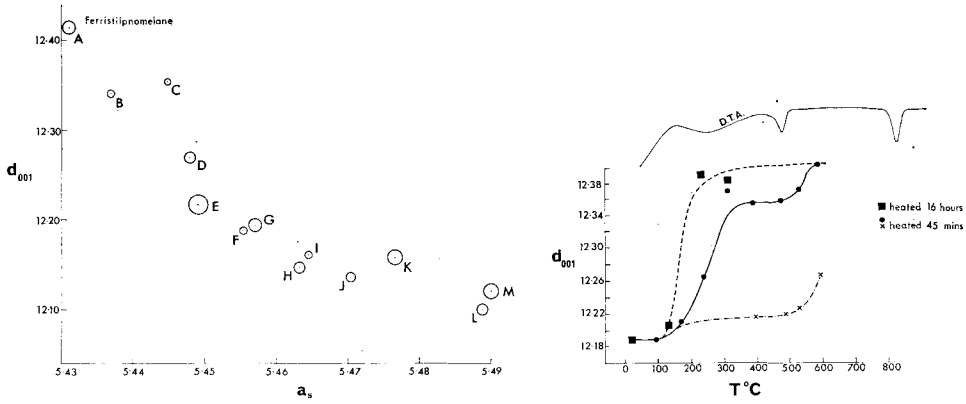

FIGS. 6 and 7: FIG. 6 (left). Plot of a *vs.* d_{001} for stilpnomelane; a_s = subcell a. Sample letters refer to Table I. Radius of circles, one standard deviation as determined from the least squares refinement. FIG. 7 (right). D.T.A. curve (upper) and plot of d_{001} against temperature for stilpnomelane F (Table I).

Unit-cell content. To determine the unit-cell content, it was assumed that no Ca, Na, or K occur in the octahedral or tetrahedral sheets. Consideration of the chemical analysis, cell volumes, and densities of the 4 stilpnomelanes A, E, H, I listed in Table III shows that there are 122 cations other than Ca, Na, K, or H, compared with 120 octahedral and tetrahedral cations of the model structure. Allocating 48 cations to the octahedral sheet (16 subcells as in Part 1) leaves 74 (Si+Al) in the double tetrahedral sheet, or 37 in each sheet. The tetrahedral sheet has trigonal symmetry, and therefore 36 tetrahedral sites have been assumed.

The discrepancy may arise from loss of water during desiccation prior to density determination, and the subsequent repenetration of water during the determination, leading to a high value for the density. Hutton (1938) has shown a weight loss of 3 % can be achieved by prolonged desiccation of stilpnomelane.

48 chemical analyses of stilpnomelane from the literature have been recalculated on the basis Si+Al+Ti+Fe+Mn+Mg = 120, and assuming that H_2O^+ and H_2O^- do not accurately represent structural and absorbed water respectively (Table IV). Allocation of cations has been made on the following basis: Si+Al = 72, excess Al in octahedral sites; octahedral (OH) = $\sum R^{2+}$ in octahedral sites; any tetrahedral charge deficiency caused by substitution of Al for Si is balanced by $(Ca+Na+K+H)^+$,

or any excess interlayer charge resulting when $(Ca+Na+K)^+ > Al^{IV}$ is balanced by $(OH)^-$; remaining H^+ is allocated as H_2O.

The range of each of the major components Si, Al, Mg, total alkalis, and H_2O was examined, and any analysis having more than 2 components at the extremes of their range was considered unrepresentative. This procedure probably excludes accurate analyses of material with the stilpnomelane structure, but as single-crystal X-ray data are not available for any stilpnomelanes with 'unrepresentative' chemistry

TABLE III. *Cell dimensions and densities of 4 stilpnomelanes. Standard deviations ($\times 10^{-3}$) are given in brackets*

Sample no. (Table I)	A	E	H	I
a	21·724(4) Å	21·796(6)	21·853(3)	21·857(2)
b	21·724(4) Å	21·796(6)	21·853(3)	21·857(2)
c	17·740(4) Å	17·633(5)	17·608(2)	17·620(1)
α	121·14°(10)	124·51(20)	124·67(10)	124·65(10)
β	95·86°(20)	95·91(30)	95·94(10)	95·93(10)
γ	120·00°(10)	120·00(20)	120·00(10)	120·00(10)
d_{001}	12·414 Å	12·217	12·147	12·161
V	5074 Å^3	5026	5023	5032
Density	2·827	2·931	2·794†	2·833†
[Si+Al+Fe+Mn+Mg]	122·6	121·6	121·1	124·5

† Data from Blake (1965).

their equivalence with stilpnomelane has not been assumed. These analyses are listed in Table IVb. Of the 37 remaining analyses (Table IVa) only 3 have insufficient Si and Al to fill the 72 tetrahedral sites (nos. 4, 16, 17), and in these the deficiency is not great.

Hashimoto (1969) observed no relation between the oxidation state of iron in stilpnomelane and $H_2O(+)$ reported in analyses. There is also no obvious relation between total H_2O and Fe^{3+}/Fe^{2+} in the 37 analyses listed here. However, if H_2O remaining after H has been allocated as above is plotted against (OH) ($= 48-R^{3+}$) a trend is quite noticeable, from about 17 H_2O in ferrostilpnomelane to about 35 H_2O in ferristilpnomelane (fig. 8).

Three pairs of analyses are available of stilpnomelane samples from the same rock with different Fe^{3+}/Fe^{2+} ratio; these pairs show the trend even more clearly (1, 2, 3, Fig. 8). Essentially such a representation of the data only shows that total hydrogen in stilpnomelane is roughly constant; however, it can be interpreted as supporting Hutton's (1938) hypothesis that oxidation of Fe^{2+} is achieved at the expense of octahedral hydrogen. The mechanism envisaged here is that as the availability of oxygen increases (e.g. by exposure to weathering) oxygen permeates the stilpnomelane structure through the large channels in the tetrahedral sheet (2·4 Å minimum). Fe^{2+} is then oxidized to Fe^{3+} and the hydrogen so released from the octahedral anions combines with the oxygen to form water, which remains in the cavities in the tetrahedral sheet in much the same way as zeolitic water.

TABLE IVa. *Representative stilpnomelane structural formulae*

	1	*2*	*3*	*4*	*5*	*6*	*7*	*8*	*9*	*10*	*11*	*12*	*13*	*14*	*15*	*16*	*17*	*18*	*19*
Si	62·3	62·8	62·9	62·0	64·3	62·1	62·7	65·7	61·1	63·2	65·0	59·9	65·5	57·1	64·8	63·9	62·7	65·3	61·4
Al^{iv}	9·7	9·2	9·1	7·8	7·7	9·9	9·0	6·3	10·9	8·5	7·0	12·1	6·5	14·9	7·2	6·7	8·5	6·7	10·6
Fe^{iv}	—	—	—	2·2	—	—	0·3	—	—	0·3	—	—	—	—	—	1·4	0·8	—	—
Al^{vi}	0·6	2·6	1·0	—	4·4	2·9	—	4·2	3·2	—	1·9	0·3	1·9	5·1	0·4	—	—	1·7	1·1
Ti	—	0·2	0·1	—	—	0·1	—	0·2	—	0·2	—	0·1	—	—	0·1	0·1	0·2	—	0·2
Fe^{3+}	3·4	2·2	4·9	7·4	3·2	4·8	10·1	4·2	5·9	9·2	8·4	10·1	8·9	7·4	12·1	13·1	16·5	18·8	20·1
Fe^{2+}	27·9	30·9	29·7	36·8	24·2	31·2	26·6	26·2	22·3	34·5	28·9	27·1	28·8	21·7	23·1	30·4	17·7	19·2	10·3
Mn	—	0·4	0·4	—	—	0·3	8·3	3·1	0·5	0·1	0·7	0·3	1·0	0·6	0·4	0·1	1·3	0·5	3·4
Mg	16·0	11·7	11·9	3·8	16·2	8·7	5·0	10·1	16·0	4·1	8·1	10·1	7·4	13·1	11·9	4·3	12·3	7·8	12·8
Ca	n.d.	1·1	0·4	—	4·3	—	—	1·2	1·9	0·8	0·7	—	0·5	3·0	1·4	0·6	—	0·4	0·7
Na	1·5	1·7	1·4	4·2	4·3	1·6	0·3	—	—	1·1	0·4	1·4	—	—	0·7	1·9	2·3	0·2	2·3
K	6·0	2·7	2·6	2·0	2·7	2·7	2·1	1·4	3·7	0·8	3·3	2·7	2·3	5·0	3·6	4·1	3·2	2·6	0·6
$(OH)^-$	44·0	42·9	42·0	40·7	40·4	40·1	39·9	39·1	38·8	38·6	37·7	37·4	37·2	35·5	35·2	34·7	31·3	27·5	26·3
H^+	2·3	2·6	4·3	3·7	—	5·6	5·9	2·4	3·3	5·2	2·0	6·7	3·2	4·0	0·0	0·9	3·8	3·0	6·2
H_2O	20·0	19·5	19·0	33·6	19·7	21·9	21·6	22·8	14·2	22·9	19·1	23·7	14·5	13·1	17·3	23·7	24·5	24·6	26·0

	20	*21*	*22*	*23*	*24*	*25*	*26*	*27*	*28*	*29*	*30*	*31*	*32*	*33*	*34*	*35*	*36*	*37*	Ave.
Si	63·4	64·1	63·1	62·6	61·7	63·2	63·6	62·2	65·5	65·3	65·2	63·5	61·2	60·0	62·7	62·7	60·8	63·8	63·0
Al^{iv}	8·6	7·9	8·9	9·4	10·3	8·8	8·4	9·8	6·5	6·7	6·8	8·5	10·8	12·0	9·3	9·3	11·2	8·2	9·0
Fe^{iv}	—	—	—	—	—	—	—	—	—	—	—	—	—	—	—	—	—	—	—
Al^{vi}	1·9	1·0	3·2	1·3	2·6	1·0	3·0	1·1	1·8	8·3	2·7	0·2	3·1	14·6	2·7	2·2	0·1	3·5	2·3
Ti	—	0·1	—	—	—	—	—	0·3	0·2	—	—	0·1	0·7	—	0·1	0·2	—	—	0·1
Fe^{3+}	22·1	23·4	22·2	24·2	23·4	25·0	23·6	26·2	25·9	20·0	26·0	28·4	24·3	16·3	29·0	30·3	35·8	33·8	35·5
Fe^{2+}	15·2	20·0	16·6	18·8	15·9	7·4	16·3	4·0	15·9	7·9	10·8	3·5	4·9	13·8	3·9	1·2	1·0	1·5	
Mn	0·3	0·4	0·1	0·6	0·1	0·8	0·1	0·7	0·1	0·8	1·4	3·3	0·9	—	0·5	3·2	0·3	3·1	0·8
Mg	8·4	3·1	5·9	3·1	6·0	13·8	4·9	15·7	4·1	10·9	7·1	12·5	14·0	3·3	11·8	10·9	10·8	6·1	9·3
Ca	0·1	—	0·8	0·8	1·4	0·4	1·3	2·8	1·0	1·9	6·6	1·3	1·5	1·9	0·3	1·0	—	0·5	1·1
Na	0·2	3·8	0·1	n.d.	0·3	0·3	—	0·1	0·2	0·9	n.d.	1·5	1·2	0·8	0·9	3·5	—	1·1	1·2
K	6·0	2·4	3·7	1·4	3·5	3·2	2·5	2·9	0·9	3·0	n.d.	1·3	2·5	1·0	3·2	0·7	—	1·6	1·5
$(OH)^-$	23·9	23·4	22·6	22·5	22·0	22·0	21·3	20·0	19·9	20·7	25·7	19·1	19·1	17·1	16·1	15·2	12·1	10·7	
H^+	2·2	1·6	3·5	6·4	3·7	4·4	3·4	1·2	3·4	—	—	3·0	4·0	6·3	4·5	3·1	11·2	4·5	79
H_2O	22·9	29·8	23·6	28·2	29·7	24·5	27·0	23·7	32·5	7·6	25·1	31·2	37·5	21·3	33·9	29·0	35·0	32·0	

TABLE IVb. *Non-representative stilpnomelane structural formulae*

	38	*39*	*40*	*41*	*42*	*43*	*44*	*45*	*46*	*47*	*48*	*49*
Si	64·0	63·2	54·2	61·3	61·5	62·2	57·5	60·7	63·0	50·2	66·2	57·6
Al^{iv}	6·7	7·6	15·6	7·8	7·7	9·8	14·3	10·0	9·0	21·8	1·8	12·1
Fe^{iv}	0·4	0·4	2·2	3·0	2·8	—	0·1	1·4		—	4·0	2·3
Al^{vi}	—	—	—	—	—	5·6	—	—	2·3	6·6	—	—
Ti	—	—	—	—	—	—	0·7	—	—	0·1	—	—
Fe^{3+}	—	—	1·8	2·6	4·4	2·4	6·8	22·6	25·0	20·4	31·8	31·5
Fe^{2+}	41·9	n.d.	30·2	27·1	8·3	24·9	22·6	6·7	—	13·4	11·2	7·2
Mn	1·8	42·9	0·4	1·0	7·2	0·6	3·6	—	—	—	3·3	4·2
Mg	5·1	5·9	15·6	17·3	23·1	14·4	14·2	18·7	20·7	7·4	1·6	5·1
Zn	—	—	—	—	5·0	—	—	—	—	—	—	—
Ca	—	—	0·1	—	0·8	n.d.	1·3	n.d.	n.d.	2·9	3·3	5·4
Na	0·3	0·6	0·3	—	1·0	n.d.	—	n.d.	n.d.	1·7	0·5	0·3
K	3·6	1·8	12·3	—	4·8	n.d.	5·7	n.d.	n.d.	1·8	0·8	0·2
$(OH)^-$	48·7	48	46·0	45·4	43·6	40·0	39·7	25·4	20·7	20·7	16·1	16·5
H^+	4·1	6·5	—	10·7	3·0	?	6·2	?	?	12·5	—	3·2
H_2O	0·2	35·7	—	29·8	15·1	25·4	13·5	28·2	53·0	5·3	38·9	72·0

References to analyses in Table IV. Author, reference if not listed with main references, analyst if not the first author, author's analysis no. (in parentheses), analysis no. in Table IV.

Agrell *et al.*, 1965. (Zussmanite). 38.
Ayres (V. L.), 1940. *Amer. Min.* **25,** 432. 36.
Blake (R. L.), 1965. (D. Thaemlitz, B.M. 85, B.M. 107), 11, 18; (E. H. Oslund, B.M. 95), 13.
Epprecht (W.), 1946. [*Schweiz. Min. Petr. Mitt.* **26,** 19]; M.A. **10**–226. (Jakob), 4.
Frondel (C.), and Ito (J.), 1965. *Amer. Min.* **50,** 498. (Ito), 42.
Gay (M.), 1966. *Bull. Soc. franç. Min. Crist.* **89,** 344. (M. C. Fournier), 29.
Grout (F. F.) and Thiel (G. A.), 1924. *Amer. Min.* **9,** 228. (Grout), 15.
Gruner (J. W.), 1937. (S. Goldich), 20.
Häberle (H.), 1969. (A), 33; (B), 47.
Hallimond (A. F.), 1924. *Min. Mag.* **20,** 193. (F. R. Ennos), 23.
Hashimoto (M.), 1968. *Journ. Fac. Sci. Univ. Tokyo*, II, **17,** 99, (H. Haramura), 32.
Holzner (J.), 1933 [*Neues Jahrb. Min., Abt. A, Beil.-Bd.* **66,** 213]; M.A. **5**–286. 16.
Hutton (C. O.), 1938. (C), 8; (D), 22; (F), 24; (E), 26; (B), 27; (G), 37.
—— 1945. *Amer. Min.* **30,** 714. 34.
—— 1956. Ibid. **41,** 608. (A), 19; (B), 35; (R. Klemens, C), 31.
Jakob (J.), 1923. [*Schweiz. Min. Petr. Mitt.* **3,** 227]; M.A. **2**–251. (Parsettensite), 39.
—— 1927. [Ibid. **7,** 311]; quoted in Gruner (1937), 17.
Kräutner (H. G.) and Medeşan (A.), 1969. (3), 9; (1), 14; (2), 44.
LaBerge (G. L.), 1966a. *Econ. Geol.* **61,** 147. (R. L. Bruce), 1.
—— 1966b. Ibid. 572. (Geol. Surv. Canada), 40.
[Lazarenko (E. K.)] Лазаренко (Е. К.), 1954. [Мин. сборн. Львов. геол. общ. (*Min. Mag. Lvov Geol. Soc.*), **8,** 119]; M.A. **13**–61. (1), 5; (2), 43.
Matthews (D. W.) and Scoon (J. H.), 1964. *Min. Mag.* **33,** 1032. (J. H. Scoon) 1, 2, 10, 28.
[Mozgova (N. N.)] Мозгова (Н. Н.), 1957 [Мин. сборн. Львов. геол. общ. (*Min. Mag. Lvov Geol. Soc.*) **11,** 273]; M.A. **14**–272. 49.
Rayner (E. O.), Geol Surv. N.S.W., unpubl. (S. H. Pyle), 21.
Read (P.), priv. comm. (J. A. Maxwell), 25.
Shannon (E. V.), 1921. *Proc. U.S. Nat. Mus.* **57,** 397. (Ave. of I and II), 41; (chalcodite), 46.
—— 1921. Ibid. **58,** 451. 45.
Shirozu (H.), 1955. *Kobutsugaku zasshi*, **2,** 115. 48.
—— 1964. *Sci. Rep. Fac. Sci. Kyushu Univ., Geol.*, **7,** 99. 7.
Wager (L. R.), and Deer (W. A.), 1939. *Medd. Grønland*, **105,** no. 4, 188. 30.
Yui (S.), 1962. *Journ. Geol. Soc. Japan*, **68,** 597. (H. Haramura, 59025), 2; (56034(a)), 3; (57053), 6; (56034(b)), 12.

Hashimoto also observes that stilpnomelane analyses fall into two groups, one with $Fe_2O_3/(Fe_2O_3+FeO) < 0{\cdot}3$, the other with this ratio $> 0{\cdot}6$. An explanation for this distribution of R^{3+} and R^{2+} can be found by examination of the environment of the 48 octahedral cations. The anion octahedra surrounding 18 of these cations share 4 oxygens with silicon, a further 18 share 3 oxygens with Si, 8 share 2 oxygens, 2 share 1 and 2 share no oxygens. If it is assumed that the proximity of a silicon cation will inhibit oxidation of Fe^{2+} because of cation repulsion and local charge

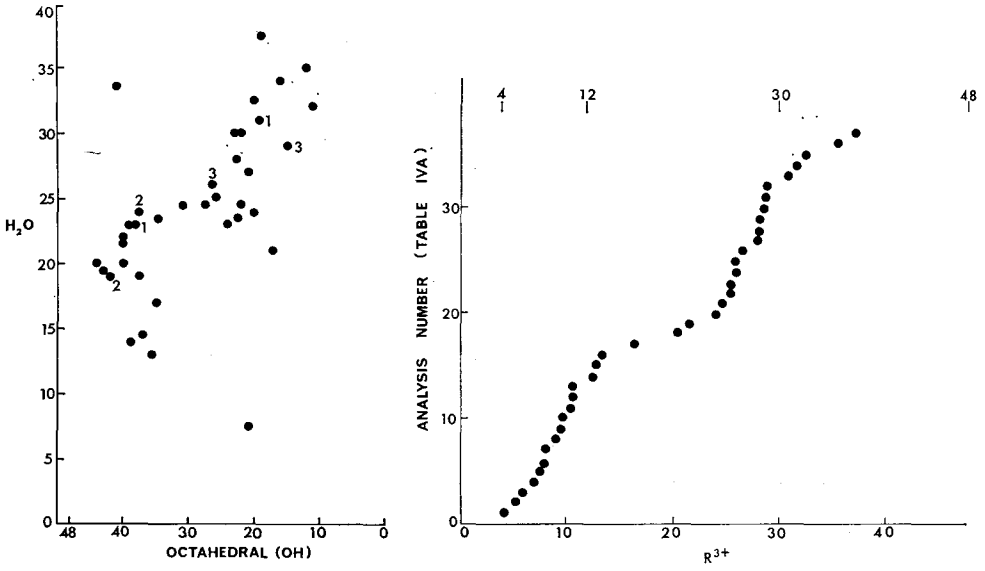

FIGS. 8 and 9: FIG. 8 (left). Plot of H_2O *vs.* octahedral (OH) for stilpnomelanes listed in Table IV. FIG. 9 (right). Cumulative plot of octahedral R^{3+} cations in stilpnomelanes. Breaks in slope correspond with the numbers of cations in the four different environments.

imbalance on the shared oxygen, then one would expect up to 4 trivalent cations to be readily accommodated in the octahedra sharing none or 1 oxygen with silicon, and that oxidation of a further 8 ferrous iron cations (sharing 2 oxygens with silicon) would be relatively easy. To oxidize further cations would require the oxidation potential to increase sufficiently to overcome the energy barriers, whereupon oxidation of a further 18 cations (sharing 3 oxygens with silicon) would occur. Even higher oxidation potentials would be needed to oxidize the remaining ferrous iron cations. These effects are shown in fig. 9 where the distribution of trivalent cations is shown as total R^{3+} *vs.* number of analyses. The bulk of the analyses have R^{3+} ranging from 4 to 12 or from 24 to 30. The gap between $R^{3+} = 12$ and 24 arises because if the oxidation potential is sufficient to oxidize any of the Fe^{2+} cations sharing 3 oxygens with Si, it is sufficient to oxidize most or all of them.

Interpretation of T3 reflections. The intensities of the 'T3 reflections' produced optically from the ideal model are practically zero, in contrast to the high measured values of the T3 X-ray reflections.

The fact that the T2 and T3 reflections can be distinguished from each other suggests they arise in different ways. The T3 reflections appear as satellites to the rows of T1 reflections parallel to c^* and can be explained in terms of deviations in the z-direction from the positions of subcell lattice points. The x- and y-co-ordinates of the iron atoms in the full cell are at intervals of one twelfth. A periodic displacement in the z-direction repeating every 12 atoms as in fig. 10 introduces significant intensity only at the positions of the T1 and T3 reflections.

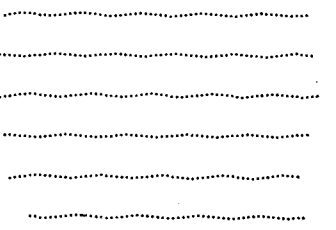

FIG. 10. Diffraction mask representing the warping of the planes of octahedral cations.

Refinement. The ideal model with planar octahedral and tetrahedral sheets has a theoretical layer thickness of about 11 Å, significantly less than the observed value of 12·4 Å. Furthermore, while there is qualitative agreement between observed and calculated intensities for the T2 reflections, there is no agreement for the T3 reflections.

The 'islands' of 24 tetrahedra have a diameter (at the apical oxygens) of about 15·2 Å, whereas the equivalent region of an ideal octahedral sheet has a diameter of about 16·1 Å. The octahedral–tetrahedral junction will therefore warp into a saucer shape, and so increase the layer thickness. The warping of the planes of atoms produces the T3 reflections.

A Fourier synthesis using phases derived from this model showed that the bases of the tetrahedra of the 6-member rings linking the 'islands' are not flat, but tilted somewhat. Such a tilt further increases the thickness of the layer.

Further refinement is severely hampered by the large number of atoms in the unit cell, and by the comparatively few superlattice reflections that are observable (superlattice points exceed sublattice points by a factor of 16, but less than half the observable reflections are T2 and T3 reflections). Some degree of refinement was achieved using least-squares methods, but with severe limitation on the variables. The x- and y-co-ordinates of all atoms were kept constant (relative to an axis normal to the ab-plane, passing through the centre of an 'island'). The atoms of the saucer-shaped regions of the octahedral and tetrahedral layers were then grouped as concentric rings of atoms with common z-co-ordinate. The iron atoms at $z = 0{\cdot}5$ and the oxygens at $z = 0$ were held to those co-ordinates. The 16 groups so obtained are listed in Table V. The same value for the isotropic temperature factor was assumed for all atoms of a given plane (in the ideal unwarped model). Two scale factors were applied to each level of data collected, one for the sharp T1 and T3 reflections, a second for the diffuse T2 reflections.

There were thus 34 variables for 168 atoms with 674 observed reflections. The restrictions placed on the co-ordinates prevent any detail in the structure being determined, and so the reflections were given weight $1-(\sin\theta)/\lambda$ to reduce the effect of the high angle reflections, which are sensitive to small errors in x, y, and z.

This model refined from an initial R of 50 % to an over-all R (including unobserved reflections) of 21 %, weighted $R = 20{\cdot}5$ %. Considering that the error in

measurement of the streaked T2 reflections may be as large as 25 %, and that none of the water molecules (presumably within the tetrahedral sheet) were included in the model, the agreement between observed and calculated structure factors is satisfactory. The structure is drawn in figs. 11 and 12.

TABLE V. *Atomic co-ordinates from least-squares refinement (standard deviations in parentheses)*

	Number	*z*	*B*
Fe	6	0·533(1)	3·0(1)
	6	0·521(2)	
	12	0·5	
Si (island)	6	0·301(3)	3·6(3)
	6	0·286(3)	
	12	0·272(2)	
Si (6-member ring)	6	0·132(2)	2·7(7)
Oxygens (octahedral)	13	0·437(3)	3·6(3)
	26	0·419(2)	
	9	0·400(4)	
Oxygen (basal)	6	0·269(6)	4·2(5)
	6	0·266(7)	
	18	0·240(3)	
	12	0·205(4)	
	12	0·153(4)	
Oxygens (6-ring apical)	6	0·0	8·8(19)

Discussion

Structural variation with composition. The variations in cell dimension shown in fig. 6 can be generally explained in terms of the structure. No attempt has been made to derive a rigorous relation between cell dimension and composition, as only 6 of the samples used were separates from analysed material.

The largest observed *a* of 21·96 Å is for ferrostilpnomelane from the Hamersley Ranges. This value is about 2 % smaller than the equivalent distance in the ferrous iron silicate zussmanite (22·34 Å); the reduction is probably caused by incorporation of some smaller cations (Al, Fe^{3+}, Mg) in the octahedral sheet and by the greater constraint imposed on this sheet by the islands of 24 tetrahedra in stilpnomelane than by the 6-member rings in zussmanite. The decrease in *a* with increasing ferric iron is too small to be explained by simple geometry based on the size of Fe^{2+} and Fe^{3+} ions; however, one would expect that the increased cation repulsion caused by oxidation would to some extent offset contraction caused by a decrease in ionic radius.

The tetrahedral sheet can adjust to variations in octahedral sheet dimensions by movement of the paired rings of 6 tetrahedra connecting the 'islands'. Rotation of these

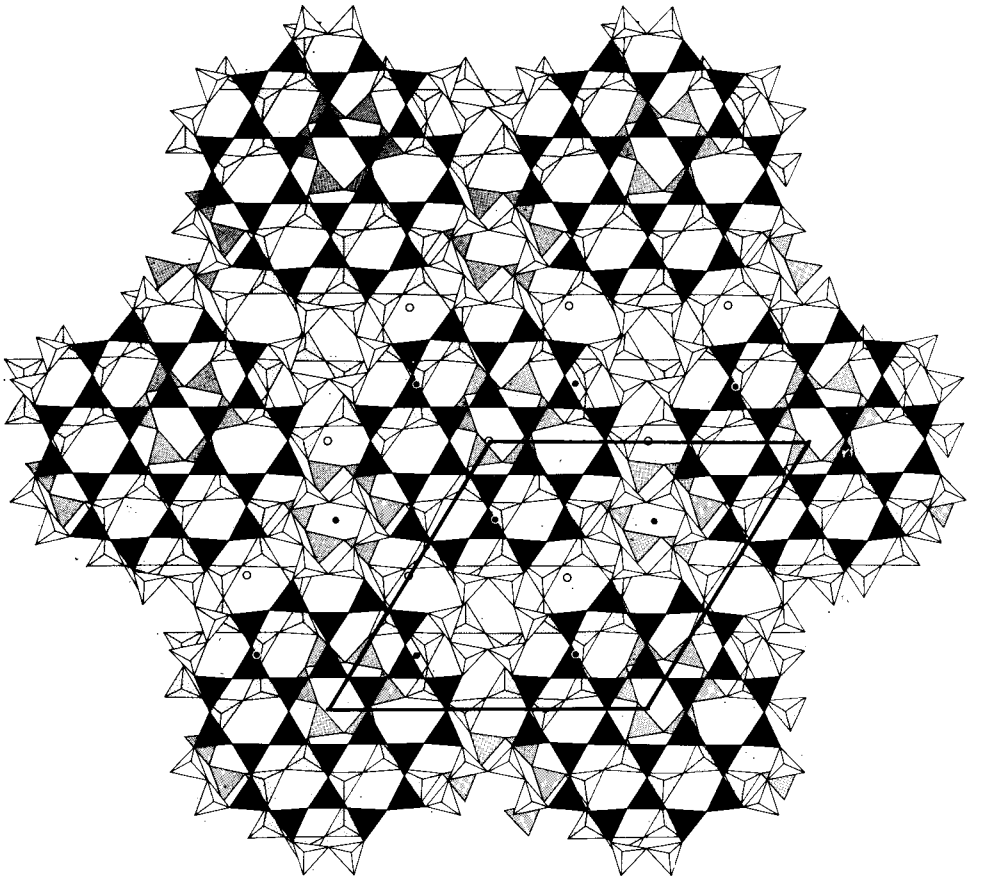

FIG. 11. Perpendicular projection of the tetrahedral sheets co-ordinating above and below an octahedral sheet. Outline tetrahedra, 6-member rings linking 'islands' above the octahedral sheet. Solid triangles, 'islands' above the octahedral sheet. Stippled tetrahedra, 'islands' below the octahedral sheet. Stippled triangles, 6-member rings linking the lower 'islands'. The octahedral cations are not shown. The outline cell shows a and b at $z = 0$. Open circles, centres of symmetry at $z = 0$. Full circles, centres of symmetry at $z = \frac{1}{2}$.

tetrahedra in the *ab*-plane can vary the ring from di-trigonal to hexagonal, giving a range for a of from 21·1 Å to 22·3 Å (assuming a tetrahedral O–O distance of 2·64 Å). Alternately, the tetrahedra of the 6-member rings can tilt to make one edge more nearly vertical. Such a rotation reduces a and increases d_{001}, each by a maximum of 0·5 Å as the tetrahedra move from having their bases horizontal to having one edge vertical.

It is suggested therefore, that in the early stages of oxidation, the 6-member rings twist about 2° in the *ab*-plane, reducing a from 22·0 Å to about 21·8 Å, and tilt about 2°, increasing d_{001} by 0·1 Å. As oxidation increases, loss of H^+ from the octahedral layer increases anion repulsion between the oxygens of the octahedral layer

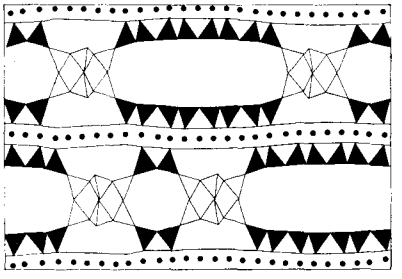

FIG. 12. [110] projection of a slab of the stilpnomelane structure through the 6-member rings and the centres of 'islands'. Solid triangles, 'island' tetrahedra; circles, octahedral cations.

and of the 6-member rings, accelerating the tilting of these tetrahedra. A total rotation of 3° and a tilt of 10° is adequate to explain the observed variation in cell dimension. Fig. 13 shows these changes diagrammatically.

Figure 6, which shows the variation of a and d_{001} for various stilpnomelanes, can be interpreted to show the point at which the tetrahedral sheet adjustment changes from being predominantly a twist in the ab-plane to being a tilt. If the data are regarded as lying on 2 straight line segments, an inflection point occurs midway between samples F and G and samples H and I. Sample G has 20 R^{3+} cations,

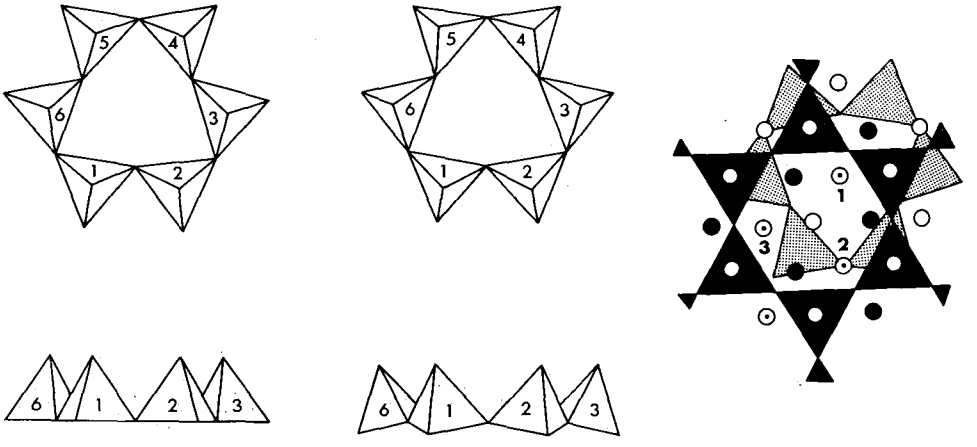

FIGS. 13 and 14: FIG. 13 (left). 6-member rings. Above, plan; below, section. Left, ferrostilpnomelane; right, ferristilpnomelane. FIG. 14 (right). Detail showing the three possibilities for the superposition of the 6-member rings (stippled) on the central hexagonal 'islands'. The centre of the 6-member ring can adopt position 1 or positions 2 or 3 with equal ease. Octahedral cations, full circles; octahedral anions, open circles.

and falls on the ferristilpnomelane side of the composition gap shown by Hashimoto (1969) and explained above, whereas samples H and I with about 11 R^{3+} cations are ferrostipnomelanes. Thus the compositional gap may have an associated structural change.

Cell shape. The triclinic shape of the unit cell of stilpnomelane is a further result of the misfit between tetrahedral and octahedral sheets. In order to accommodate the smaller tetrahedral sheet, the octahedral sheet warps slightly, being concave toward the 'islands' of 24 tetrahedra. As a result, two 'islands' cannot co-ordinate opposite on either side of the octahedral sheet, and so each 'island' is opposed by a trigonal ring. The centres of the 'islands' and of the trigonal rings are offset in vertical

projection, because they superimpose over the octahedral anions on their respective sides of the octahedral sheet (fig. 14).

Given the position of an 'island' above the octahedral sheet, there are 3 ways the 'island' below can be positioned so that it is as near as possible to superimposing on the centre of a trigonal ring above it (i.e., so that the centre of the lower 'island' is as far away as possible from the convex warp in the octahedral sheet caused by the upper 'island', and *vice versa*). These 3 positions (marked 1, 2, 3 in fig. 14) are duplicated at the other trigonal ring, and so provide 6 possible variations in the stacking sequence for stilpnomelane layers. Random adoption of these positions by successive layers can cause the one dimensional disorder revealed by the T2 reflections from most crystals of stilpnomelane.

Despite the semirandom stacking of the tetrahedral sheets, the pattern of warping in the octahedral sheet remains regular, because the trigonal ring adopts one of 3 positions symmetrically about the pattern of warping. The T3 reflections arise largely from the octahedral sheet, and hence these are sharp reflections.

Comparison with zussmanite. Zussmanite occurs with stilpnomelane in the Laytonville quarry in Mendocino County, California (Agrell *et al.*, 1965); its unit cell contains $A_1 R^{vi}_{13} T^{iv}_{18}(O,OH)_{56}$, or very close to $\frac{1}{4}$ of the full stilpnomelane unit cell ($A_1 R^{vi}_{12} T^{iv}_{18}(O,OH)_{54}$). All the elements listed in the structural formula of zussmanite fall in the observed range for each element in stilpnomelanes. The structures of zussmanite (Lopes-Vieira and Zussman, 1969) and stilpnomelane are similar, each having a discontinuous tetrahedral sheet co-ordinated to a slightly warped iron-rich octahedral sheet. It is interesting to speculate whether any of the ferrostilpnomelanes reported in the literature are actually zussmanite, and whether zussmanite and stilpnomelane are polymorphs.

Conclusion. The large unit cell of stilpnomelane (mol. wt. $\sim$ 7900) arises because there is only slight misfit between a smaller tetrahedral sheet and a larger octahedral sheet. Such effects have been noted for the pyroxenoids and are becoming evident for the layer silicates. Stilpnomelane is unique in permitting substitution of Fe^{3+} for Fe^{2+} to the extent of 2 out of 3 octahedral cations. This is possible for two reasons, both considered necessary; first, only one-third of the octahedra surrounding the iron, atoms co-ordinate to 4 tetrahedra (compare all octahedra in, say, biotite), hence oxidation of the remaining two-thirds of the octahedral cations is electrostatically feasible, and second, the tetrahedral sheet is hinged in such a way that it can expand and contract to accommodate varying octahedral sheet dimensions.

The actual ratio of Fe^{2+} to Fe^{3+} shown by a particular stilpnomelane appears to depend on the oxidation–reduction conditions obtaining at the place of collection of the sample. From a structural point of view, both ferro- and ferristilpnomelane appear equally stable given appropriate oxidation conditions; there seems to be no reason to assume that all ferristilpnomelane forms by oxidation of earlier ferrostilpnomelane. Field evidence certainly indicates that ferrostilpnomelane can be a primary phase, for example in the banded iron formation of the Hamersley Ranges, Western Australia (LaBerge, 1966), and that ferristilpnomelane can result from the alteration

of ferrostilpnomelane (Hutton, 1938). On the other hand some vein stilpnomelanes are ferristilpnomelanes and show no evidence of ever having been ferrostilpnomelane (e.g. Table IV analyses 18, 21, 36). Zen (1960) argues that the identity of structural role played by Fe^{2+} and Fe^{3+} is evidence that Fe^{3+} is oxidized Fe^{2+}. It could equally be argued that Fe^{2+} is reduced Fe^{3+}. The ease with which ferrostilpnomelane oxidizes makes it very difficult to be certain that a particular ferristilpnomelane has not undergone alteration. Until more information is available on 'fresh' ferristilpnomelane, its status as a primary mineral in metamorphic rocks remains uncertain.

Acknowledgements. This study was begun under the support of the National Science Foundation's Grant GP-3748 (Bailey). Acknowledgement is also made to the donors of the Petroleum Research Fund, administered by the American Chemical Society, for partial support of this research under grant PRF 4899-AC2 (Bailey). The work owes much to the encouragement and advice of many people, particularly Dr. S. W. Bailey who initiated the project, and Dr. A. J. R. White who suggested many fruitful lines of thought. Discussions with Drs. B. W. Chappell, A. E. Grady, I. M. Threadgold, and B. Gunthorpe have also proved invaluable. Dr. P. Read kindly provided unpublished analytical data.

Sincere thanks are due to Mr. G. Lea for his work in preparing detail designs and in construction of the pantograph punch. Mr. J. Pennington performed the D.T.A. experiments and prepared some of the powder diffraction photographs, Mr. B. Wight reproduced the diffraction photographs for publication. The computations were carried out at the A.N.U. Computer Centre, the assistance of the Centre Staff is gratefully acknowledged.

My deepest appreciation goes to my wife for her patience and encouragement over the years she has had to live with a mineral that does not even have the virtue of being pronounceable.

REFERENCES

AGRELL (S. O.), BOWN (M. G.), and MCKIE (D.), 1965. Deerite, howieite, and zussmanite, three new minerals from the Franciscan of the Laytonville District, Mendocino Co., California. *Min. Mag.* **35,** liv; *Amer. Min.* **50,** 278.

BLAKE (R. L.), 1965. Iron phyllosilicates of the Cuyuna district in Minnesota. *Amer. Min.* **50,** 148 [M.A. **17**–299].

BROWN (E. H.), 1967. The Greenschist Facies in Part of Eastern Otago, New Zealand. *Contr. Min. Petr.* **14,** 259.

EGGLETON (R. A.), 1969. Phase determination for pseudo-symmetric centro-symmetric crystals. *Acta Cryst.* **A25,** 543.

—— 1970. Silicon tetrahedral sheet in stilpnomelane. *Nature,* **225,** 625.

—— and BAILEY (S. W.), 1965. The crystal structure of stilpnomelane. Part I. The Subcell. *Clays Clay Min.* **13,** 49 [M.A. **17**–732].

GRUNER (J. W.), 1937. Composition and structure of stilpnomelane. *Amer. Min.* **22,** 912 [M.A. 7–93].

HÄBERLE (H.), 1969. Die Stilpnomelan-Mineralien und ihr Vorkommen in Österreich. *Tschermaks Min. Petr. Mitt.* 3rd ser., **13,** 85.

HASHIMOTO (M.), 1969. A note on stilpnomelane mineralogy. *Contr. Min. Petr.* **23,** 86.

HOWELLS (E. R.), PHILLIPS (D. C.), and ROGERS (D.), 1950. The probability distribution of X-ray intensities, II, Experimental investigation and the X-ray detection of centers of symmetry. *Acta Cryst.* **3,** 210.

HUTTON (C. O.), 1938. The stilpnomelane group of minerals. *Min. Mag.* **25,** 172.

KATADA (M.) and SUMI (K.), 1966. Stilpnomelane co-existing with biotite in a Ryôke metamorphic rock. *Jour. Geol. Soc. Japan,* **72,** 517 [M.A. **19**–137].

KRÄUTNER (H. G.) and MEDEŞAN (A.), 1969. On stilpnomelane in some Romanian Carpathian Crystalline Formations. *Tschermaks Min. Petr. Mitt.* 3rd ser. **13,** 203.

KUNZE (G.), 1956. Die gewellte Struktur des Antigorits, I. *Zeits. Krist.* **108,** 82.

LaBerge (G. L.), 1966. *Eccon. Geol.* **61**, 147 and 572.
Lopes-Vieira (A.) and Zussman (J.), 1969. Further detail on the crystal structure of zussmanite. *Min. Mag.* **37**, 49.
Rost (F.) and Stettner (G.), 1969. Über Stilpnomelan in der Grünschieferzone der Münchberger Gneismasse. *Contr. Min. Petr.* **24**, 66.
Smith (M. L.) and Frondel (C.), 1968. The related layered minerals ganophyllite, bannisterite, and stilpnomelane. *Min. Mag.* **36**, 893 [M.A. **19**–314].
Taylor (C. A.) and Lipson (H.), 1964. Optical Transforms. G. Bell and Sons Ltd., London.
Zen (E-An), 1960. Metamorphism of the Lower Paleozoic rocks in the vicinity of the Taconic Range in West-Central Vermont. *Amer. Min.* **45**, 129.

[*Manuscript received 11 March 1971*]